*Korean J. Chem. Eng.*, 40(7), 1699-1708 (2023)
DOI: 10.1007/s11814-023-1382-6

pISSN: 0256-1115
eISSN: 1975-7220

# Effects of operation conditions on absorption of nitric oxide and sulfur oxide using $Fe(II)EDTA^{2-}$ absorbents

**Yoon Hee Kim*, Jiyull Kim*, Na Yeon Kim*, Dong Seop Choi*, Dong Hun Lee*, Eunju Yoo*, Young Eun Kim*, Jongwon Choi**, and Ji Bong Joo*,†**

*Department of Chemical Engineering, Konkuk University, 120 Neungdong-ro, Gwangjin-gu, Seoul 05029, Korea
**Korea Institute of Energy Research (KIER), 152, Gajeong-ro, Yuseong-gu, Daejeon 34129, Korea
(*Received 29 October 2022 • Revised 13 December 2022 • Accepted 20 December 2022*)

**Abstract**−We report simultaneous removal of NO and $SO_2$ by $Fe(II)EDTA^{2-}$ absorbent in a wet absorption system. Effects of various operation parameters, such as $Fe(II)EDTA^{2-}$ concentration, solution volume, NO inlet concentration, and pH of absorption solution on NO absorption in a semi-batch reaction, were investigated. NO loading capacity increased with increasing NO inlet concentration since NO loading capacity was highly influenced by NO inlet concentration. NO loading capacity increased in neutral and alkaline environments compared to that in an acidic one. To evaluate NO absorption performance of practical flue gas components, simultaneous absorption of NO and $SO_2$ in the presence of $O_2$ over $Fe(II)EDTA^{2-}$ was carried out. As a result, when all gas emission components (NO, $SO_2$ and $O_2$) were introduced, simultaneous removal of NO and $SO_2$ was obtained with a high NO loading capacity (ca. 88.8%). Antagonistic effects of both $SO_2$ and $O_2$ played an essential role in the regeneration of $Fe(III)EDTA^{-}$ and $Fe(II)EDTA\text{-}NO^{2-}$ to $Fe(II)EDTA^{2-}$, keeping a neutral pH of absorption solution and resulting in a dramatic improvement in the absorption of NO and $SO_2$.

Keywords: Wet Absorption, Nitric Oxide, Sulfur Dioxide, $Fe(II)EDTA^{2-}$

## INTRODUCTION

Fine dust is well known as a respirable dust that floats in the atmosphere. Harmful secondary fine dust is produced by photochemical reactions of precursor substances, such as nitrogen oxides (NOx) and sulfur oxides (SOx) in the atmosphere. Both NOx and SOx are emitted in a gaseous state from emission sources, such as power plant facilities that burn fossil fuels such as coal, natural gases, and diesel for energy generation. NOx and SOx in a gaseous state can be converted to secondary ultrafine dust such as ammonium nitrate and ammonium sulfate through photochemical reactions, causing not only serious environmental problems such as photochemical smog, air pollution, acidic rain, and ozone depletion, but also human respiratory disease [1,2]. Therefore, it is essential to remove the precursor substance of secondary fine dust such as NOx and SOx emitted from exhaust gas before they are released into the atmospheric environment.

To remove NO, many techniques, such as selective catalytic reduction (SCR) [3-5], selective non-catalytic reduction (SNCR) [6,7], plasma reduction [8,9], absorption [10], and adsorption methods [11], have been widely studied and applied toward practical De-NOx processes. Both SCR and SNCR are commonly used for removal of NO by converting NO to $N_2$ with a reducing agent [3,7]. Practically, SCR is the most widely used technology for reducing NO [3-5]. It has the advantage of high NO removal efficiency. However, to achieve a high efficiency, expensive metal catalysts such as vanadium should be used [12]. High reaction temperature conditions (300-500 °C) are also required, resulting in a high operating cost. It has another risk of corrosion due to toxic reducing agent such as ammonia. Plasma reactor can also be used for NO to $N_2$ without generating any secondary pollutants. Although the plasma method has been shown to have the highest NO removal efficiency with a clean process, it has a high installation expense for treating large amounts of flue gas stream in a practical scale plant [13,14]. Wet absorption, on the other hand, is an efficient strategy for removing gaseous pollutants such as NO and $SO_2$ in mild conditions [15]. Especially, since wet absorption processes can be operated at ambient conditions, it is suitable for low temperature de-NOx. Wet absorption (wet scrubbing) methods are relatively inexpensive for installation and easy to scale up for large processes. In addition, they can remove NOx and $SO_2$ simultaneously in one-step [16,17].

It is well known that sulfur oxide ($SO_2$) is easily removed by wet flue gas desulfurization (WFGD), since it has a high solubility in water (11.28 g/100 mL) at 20 °C and 1 atm [18]. Nitrogen oxides (NOx) generated from stationary sources are almost NO components, in which NOx compositions in the flue gas stream are ca 95% NO and 5% $NO_2$ [18,19]. It is well known that NO has a relatively lower solubility in water ($5.6\times10^{-3}$ g/100 ml) at 20 °C and 1 atm than both $NO_2$ and $SO_2$ [20]. The intrinsic low solubility of NO in aqueous solution can increase mass transfer resistance and limit overall adsorption kinetic in liquid media. Thus, it is challenging to remove NO component with a wet removal strategy.

Many researchers have studied methods to enhance NO solubility using oxidants and iron-chelate chemicals for wet absorption

†To whom correspondence should be addressed.
E-mail: jbjoo@konkuk.ac.kr

of NO [15,20-23]. Oxidant agents including NaClO, $NaClO_2$, $H_2O_2$, and $KMnO_4$ can induce oxidation of NO to $NO_2$ to increase its solubility in water, resulting in removal of gaseous NO [24]. As another strategy, iron-chelate chemicals can be used for forming a nitrosyl complex as $Fe(II)EDTA^{2-}$ bond with NO [10,15,20,25-28]. Since $Fe(II)EDTA^{2-}$ has a strong complexing ability toward dissolved NO molecules, it can rapidly capture NO molecules by forming ferrous nitrosyl with the following chemical reactions:

$$NO(g) \rightarrow NO(L) \quad (1)$$

$$Fe(II)EDTA^{2-} + NO \rightarrow Fe(II)EDTA\text{-}NO^{2-} \quad (2)$$

However, $Fe(II)EDTA^{2-}$ can be easily oxidized by dissolved $O_2$ and quickly lose its complexing ability to NO [29]. In addition, since $Fe(II)EDTA\text{-}NO^{2-}$ complex has an equilibrium constant of $10^7\ M^{-1}$, it is no longer possible to make a complex with dissolved NO molecule when an equilibrium concentration of $Fe(II)EDTA\text{-}NO^{2-}$ is achieved [20]. To overcome these problems, many research groups have suggested a regeneration strategy for recovering $Fe(II)EDTA\text{-}NO^{2-}$ and $Fe(III)EDTA^-$ to original $Fe(II)EDTA^{2-}$ state by using reducing agents such as metals [17,18,30,31], $Na_2S_2O_4$ [21,22,26], and biomass [32,33]. Even though many research groups have studied regeneration strategy of $Fe(III)EDTA^-$ and $Fe(II)EDTA\text{-}NO^{2-}$ to achieve sustainable NO removal, it is still challenging to investigate NO absorption performance and characteristics of $Fe(II)EDTA^{2-}$, when other flue gas components ($O_2$, $CO_2$, $SO_2$ and NO) are coexisting. In addition, it is also necessary to figure out the absorption mechanism and interaction of the flue gas components (both NO and $SO_2$) toward $Fe(II)EDTA^{2-}$ for designing an industry scale absorption column which can be applied to practical flue gas treatment.

In this study, we tried to find optimal operation conditions for NO absorption over $Fe(II)EDTA^{2-}$ absorbent by investigating effects of $Fe(II)EDTA^{2-}$ concentration, solution volume, inlet concentration of NO, and solution pH. In addition, to evaluate adsorption performance toward both NO and $SO_2$ from practical flue gas, we investigated effects of $SO_2$ and $O_2$ on the removal of NO by $Fe(II)EDTA^{2-}$ solution. We evaluated NO loading capacity of the $Fe(II)EDTA^{2-}$ absorbent on each case. In this paper, we discuss our systematic experimental results and the potential of simultaneous removal of NO and $SO_2$ using $Fe(II)EDTA^{2-}$ absorbent, which could be one candidate for removing both NO and $SO_2$ from practical flue gas.

## EXPERIMENTAL

### 1. Materials and Chemicals

Ferrous sulfate heptahydrate ($FeSO_4 \cdot 7H_2O$), and L(+)-ascorbic acid ($C_6H_8O_6$), sulfuric acid ($H_2SO_4$, 98%) were purchased from Daejung Chemical Company. Ethylenediaminetetraacetic acid disodium salt dihydrate ($Na_2EDTA$, 99.5%) was purchased from Yakuri Pure Chemicals. Sodium hydroxide (NaOH, 98%, bead) was obtained from Samjun Chemical Company. $N_2$ (99.999%), $O_2$ (99.999%), NO (9,910 μmol/mol), and $SO_2$ (9,504.6 μmol/mol) were used. All chemicals were used as received.

### 2. NO Absorption Experiment

NO absorption experiments were conducted in a bubble batch system shown in Fig. 1 under an anaerobic condition avoiding the effect of $Fe(III)EDTA^-$. Aqueous $Fe(II)EDTA^{2-}$ solution (2.5-12.5 mM, 300 mL) was obtained by mixing $Na_2EDTA$ and $FeSO_4 \cdot 7H_2O$ in deionized water with stirring at 500 rpm. The molar ratio of EDTA to Fe(II) was 1 : 1. L(+)-ascorbic acid was added at three times larger than the molar ratio to Fe(II) concentration in the solution to prevent oxidation of Fe(II). The pH value was then adjusted with 1 M $H_2SO_4$ and 1 M NaOH solution. All absorption reactions were carried out under the same total gas flow (1 L $min^{-1}$). The concentration of NO in inlet gas stream was controlled by regulating the relative gas flow of both NO and $N_2$. Flow rates of gases (NO, $N_2$) were controlled with a mass flow controller (MFC). Effects of initial $Fe(II)EDTA^{2-}$ concentration, absorption solution volume, NO concentration of inlet gas stream, and pH value on NO absorption were systematically investigated. Experimental conditions are shown in Table 1. Inlet and outlet gas (NO and $SO_2$) concentrations were analyzed with a flue gas analyzer (Testo model 340, Germany). NO loading capacity and removal efficiency were calculated with the following equations:

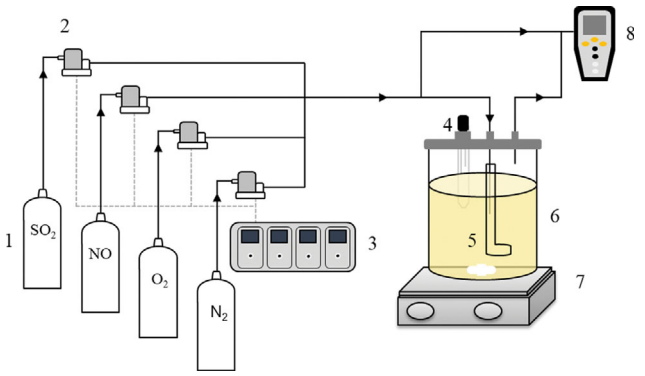


**Fig. 1. Schematic diagrams of lab-scale batch bubbler reactor for evaluating absorption performance on both NO and $SO_2$ absorption: (1) gas cylinder, (2) mass flow controller (3) control box, (4) pH meter, (5) semi-batch absorption reactor, (6) gas bubbler, (7) magnetic stirrer, (8) flue gas analyzer.**

$$\text{NO loading capacity} = \frac{n_{NO}}{n_{Fe(II)EDTA^{2-}}} \quad (3)$$

where $n_{NO}$ is the number of moles of NO absorbed (mol NO) to absorption solution, and $n_{Fe(II)EDTA^{2-}}$ is the number of initial moles of $Fe(II)EDTA^{2-}$ before absorption (mol $Fe(II)EDTA^{2-}$).

### 3. Simultaneous Absorption for Removal of Both NO and $SO_2$

To investigate effects of either $SO_2$ or $O_2$ on NO absorption, absorption experiments were conducted under the following conditions: $Fe(II)EDTA^{2-}$=10 mM, pH=6.0, V=300 ml, and 1.5 g L(+)-ascorbic acid. All absorption reactions were carried out under the same total gas flow (1 L $min^{-1}$). Concentrations of NO, $SO_2$, and $O_2$ in inlet gas stream were controlled by regulating their relative gas flow. Flow rates of the gases (NO, $SO_2$, $O_2$, $N_2$) were controlled by a mass flow controller (MFC). Inlet and outlet gas concentrations were analyzed with a flue gas analyzer Testo (Testo model 340, Germany).

### 4. Analytical Methods

The concentration of Fe(II) ions, $Fe(II)EDTA\text{-}NO^{2-}$ and Fe(III)

**Table 1. Initial experimental conditions used for NO absorption experiments**

| Serial no. | Parameter | Fe(II)EDTA$^{2-}$ | Volume | NO Inlet Conc. | pH |
|---|---|---|---|---|---|
| **1** | Fe(II)EDTA$^{2-}$ | 2.5 mM<br>5 mM<br>7.5 mM<br>10 mM<br>12.5 mM | 300 ml | 1,000 ppm | 6.0 |
| **2** | Volume | 10 mM | 100 ml<br>200 ml<br>300 ml<br>400 ml | 1,000 ppm | 6.0 |
| **3** | NO Inlet Conc. | 10 mM | 300 ml | 250 ppm<br>350 ppm<br>500 ppm<br>1,000 ppm<br>1,500 ppm | 6.0 |
| **4** | pH | 10 mM | 300 ml | 1,000 ppm | 2.0<br>4.0<br>6.0<br>8.0<br>10.0 |

EDTA$^{-}$ was estimated by using an ultraviolet/visible (UV/vis) spectrophotometer. Fe(II)EDTA$^{2-}$ was determined by following equations: (1) $C_{Fe(total)} = C_{Fe(II)} + C_{Fe(II)EDTA^{-}}$ and (2) $C_{Fe(II)} = C_{Fe(II)EDTA^{2-}} + C_{Fe(II)EDTA\text{-}NO^{2-}}$. The concentration of Fe(II) was determined by measuring absorbance at 510 nm using an ultraviolet/visible (UV/vis) spectrophotometer with the 1,10 phenanthroline colorimetry method. The standard solution of different Fe(II) concentration (0-0.15 mM) was mixed with the 1,10 phenanthroline solution containing desired concentration. Concentration of Fe(II)EDTA-NO$^{2-}$ was determined by measuring absorbance at 434 nm using an ultraviolet/visible (UV/vis) spectrophotometer. To achieve the calibration curve of concentration of Fe(II)EDTA-NO$^{2-}$, we first saturated Fe(II)EDTA$^{2-}$ (10 mM) with NO to form Fe(II)EDTA-NO$^{2-}$ and then calculated the mole number of NO adsorbed. By assuming the adsorbed NO is completely contributed to formation of Fe(II)EDTA-NO$^{2-}$, we consider that the mole of Fe(II)EDTA-NO$^{2-}$ is identical with the mole of adsorbed NO. Since Fe(II)EDTA-NO$^{2-}$ has a representative absorbance peak at 434 nm, we obtained the calibration curve by using saturated solution of Fe(II)EDTA-NO$^{2-}$. The concentration of Fe(III)EDTA$^{-}$ was determined by measuring absorbance at 225 nm with an ultraviolet/visible (UV/vis) spectrophotometer. Fe(III)EDTA$^{-}$ solution was obtained by preparing Fe(III)EDTA$^{2-}$ followed by complete oxidation processes.

## RESULTS AND DISCUSSION

### 1. Effects of Operation Parameters on NO Absorption Using Fe(II)EDTA$^{2-}$ Absorbent

Fig. 2(a) shows NO outlet concentration profiles when absorption solution is applied with different Fe(II)EDTA$^{2-}$ concentrations. When an absorption solution containing 2.5 mM Fe(II)EDTA$^{2-}$ was used, the NO outlet concentration quickly decreased from 1,009 ppm to 491 ppm. It then increased until it reached a saturation

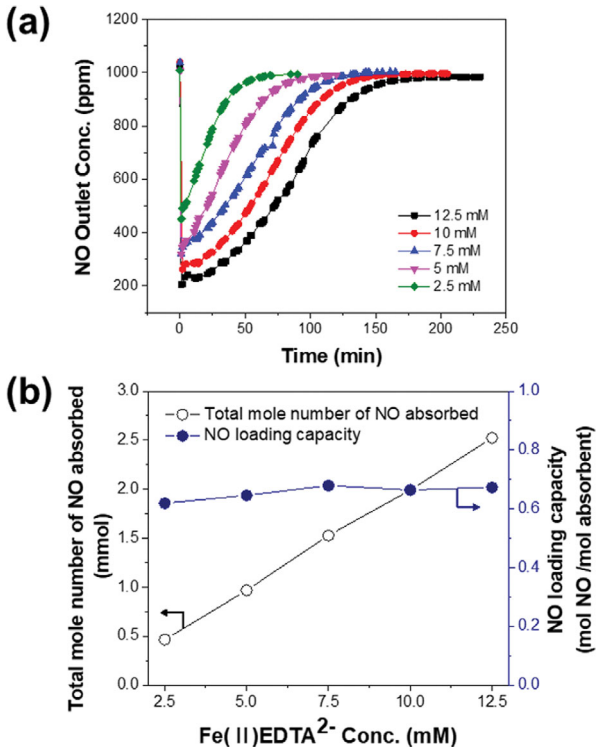


**Fig. 2. (a) NO outlet concentration profiles and, (b) Total mole number of the absorbed NO and NO loading capacity for different Fe(II)EDTA$^{2-}$ concentration (NO inlet concentration= 1,000 ppm, pH=6, V=300 ml).**

state. When the concentration of Fe(II)EDTA$^{2-}$ was increased, the lowest NO outlet value was decreased and the amount of NO absorbed was increased, although all profile patterns of NO outlet concentrations seemed to be similar. The initial lowest NO outlet concentrations were measured at 491, 344, 347, 262, and 206 ppm corresponding to initial Fe(II)EDTA$^{2-}$ concentrations of 2.5, 5, 7.5, 10 and 12.5 mM, respectively, after the absorption experiment was started. Note that the initial lowest NO outlet concentration tended to decrease with increasing Fe(II)EDTA$^{2-}$ concentration. It indicates that a higher concentration of Fe(II)EDTA$^{2-}$ can absorb more NO. When NO is absorbed in aqueous solution containing Fe(II)EDTA$^{2-}$ absorbent, NO absorption occurs by the following two chemical reactions: 1) NO+Fe(II)EDTA$^{2-}$→Fe(II)EDTA-NO$^{2-}$, 2) NO+$FeSO_4$→Fe(NO)$SO_4$. The equilibrium constant of the second reaction is K=450 $M^{-1}$, which is smaller than that of the first reaction (K=$10^6$ $M^{-1}$). Thus, NO absorption predominantly occurred by the first reaction [34]. It is well known that NO absorption in a solution containing Fe(II)EDTA$^{2-}$ occurs at the gas-liquid interface. Thus, a higher concentration of Fe(II)EDTA$^{2-}$ provides more adsorption sites near the gas (NO bubble) - liquid (absorption solution) interface. High concentrations of Fe(II)EDTA$^{2-}$ then have more chances to bind to gaseous NO molecules and capture them quickly. As NO was introduced to the absorption solution, NO outlet concentration quickly dropped. It then increased with reaction time. It means that the local concentration of Fe(II)EDTA$^{2-}$ in gas (NO bubble) - liquid (absorption solution) interface becomes lower as Fe(II)EDTA$^{2-}$ is continuously consumed for formation of Fe(II)EDTA-NO$^{2-}$, resulting in recovery of NO outlet concentration to almost its initial value.

Fig. 2(b) summarizes total mole number of NO adsorbed and NO loading capacity for different Fe(II)EDTA$^{2-}$ concentrations. As shown in Fig. 2(b), the higher the concentration of Fe(II)EDTA$^{2-}$ used, the greater the amount of NO absorbed. The slope between concentration of Fe(II)EDTA$^{2-}$ applied and total mole number of NO adsorbed was almost linear. Since we used enough amount of L-ascorbic acid in Fe(II)EDTA$^{2-}$ solution and tried to avoid any oxidant chemical to be introduced, Fe(II) was not oxidized during the whole absorption process. Thus, NO absorption mainly depends on Eq. (2) and the reaction rate can be expressed by $r=kC_{Fe(II)EDTA^{2-}}\text{-}C_{NO}$ [20]. Since we used identical concentration of NO ($C_{NO}$), the reaction rate is highly dependent on $C_{Fe(II)EDTA^{2-}}$. Thus, the total mole number of NO absorbed increased as the concentration of Fe(II)EDTA$^{2-}$ ($C_{Fe(II)EDTA^{2-}}$) increased. In addition, all concentrations of Fe(II)EDTA$^{2-}$ had similar NO loading capacity (between ca 0.62 and 0.68 mol NO/mol absorbent). This indicates that the concentration of dissolved NO is almost constant. It could be explained that NO adsorption by Fe(II)EDTA$^{2-}$ solution follows Henry's law. Since absorption conditions, such as temperature, pH, and NO concentration (partial pressure of NO), were identical for each run, Henry's constants of gaseous NO for each run were similar. It indicates that the concentration of dissolved NO is almost identical and constant. Based on the following equilibrium equations, the K′ value is almost constant. Thus, similar NO loading capacity is obtained.

$$K_{eq}=\frac{[Fe(II)EDTA\text{-}NO^{2-}]}{[Fe(II)(EDTA^{2-})][NO]} \quad (4)$$

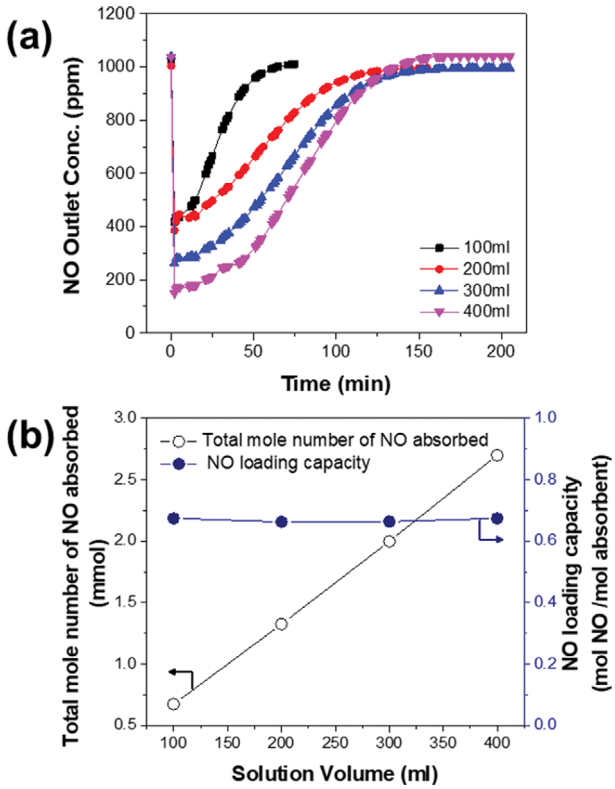


**Fig. 3. (a) NO outlet concentration profiles and, (b) Total mole number of the absorbed NO and NO loading capacity for different solution volume (NO inlet concentration=1,000 ppm, Fe(II)EDTA$^{2-}$=10 mM, pH=6).**

$$K'=K_{eq}\times[NO]=\frac{[Fe(II)EDTA\text{-}NO^{2-}]}{[Fe(II)(EDTA^{2-})]} \quad (5)$$

Thus, once an equilibrium state between the gas-liquid interface is achieved, formation of Fe(II)EDTA-NO$^{2-}$ by binding Fe(II)EDTA$^{2-}$-NO could be highly influenced by concentration of Fe(II)EDTA$^{2-}$ under the same dissolved NO concentration conditions. Higher initial concentration of Fe(II)EDTA$^{2-}$ had greater NO absorption. However, NO loading capacity for Fe(II)EDTA$^{2-}$ was almost identical at the equilibrium state for all cases.

Fig. 3(a) shows NO outlet concentration profiles when different absorption solution volumes with identical Fe(II)EDTA$^{2-}$ concentration (10 mM) are applied. Since other operation parameters, such as Fe(II)EDTA$^{2-}$ concentration, gas flow rate, and NO inlet concentration, different absorption solution volumes indicate different residence time of NO gas molecules in the absorption media. The initial lowest NO outlet concentrations were measured to be 417, 386, 262, and 150 ppm corresponding to solution volumes of 100, 200, 300 and 400 ml, respectively. It could be concluded that the lowest NO outlet values even decreased and the amount of NO absorbed increased as the absorption solution volume was increased. Since concentrations of Fe(II)EDTA$^{2-}$ and introduced NO were the same for all cases, the interface between liquid and gas in one gas bubble had an identical environment. However, the gas bubble residence time was increased with increasing reaction media volume (length). The larger the absorption solution volume, the longer the

residence time of NO molecule which can react with Fe(II)EDTA$^{2-}$ on liquid-gas interface. Thus, NO molecules have greater chance for forming Fe(II)EDTA-NO$^{2-}$. Therefore, the initial lowest NO outlet concentration decreased and the amount of NO absorbed increased with increasing solution volume.

As shown in Fig. 3(b), the total mole amount of NO adsorbed increased when the solution volume increased. The slope between absorption solution volume applied and total mole number of NO adsorbed was almost linear. Although all cases used the same concentration of Fe(II)EDTA$^{2-}$, a large volume of absorption solution indicated a large absolute mole number of Fe(II)EDTA$^{2-}$. Thus, it could be concluded that the total mole number of NO adsorbed can be linearly increased with solution volume. In addition, NO loading capacity of all solution volumes had similar values of ca. 0.66-0.67 mol NO/mol absorbent. As mentioned, NO can be absorbed on the interface between gas (NO bubble) and liquid (absorption solution). During the absorption experiment, we tried to make perfect mixing absorption solution by using a magnetic stirrer. Although there were minor differences in the concentration of Fe(II)EDTA$^{2-}$ and dissolved NO in the absorption solution, each NO bubble had an identical gas-liquid interface environment. Thus, its absorption kinetics should be similar. As absorption solution volume increased, a large amount of gas (NO bubble) - liquid (absorption solution) was formed, resulting in increased residence time for absorption of NO gas molecules. Also, the concentration of dissolved NO was the same under identical absorption conditions (same temperature, pH, and NO inlet concentration). Thus, K′ was almost constant by Eq. (6) at an equilibrium state. Therefore, NO loading capacities were similar.

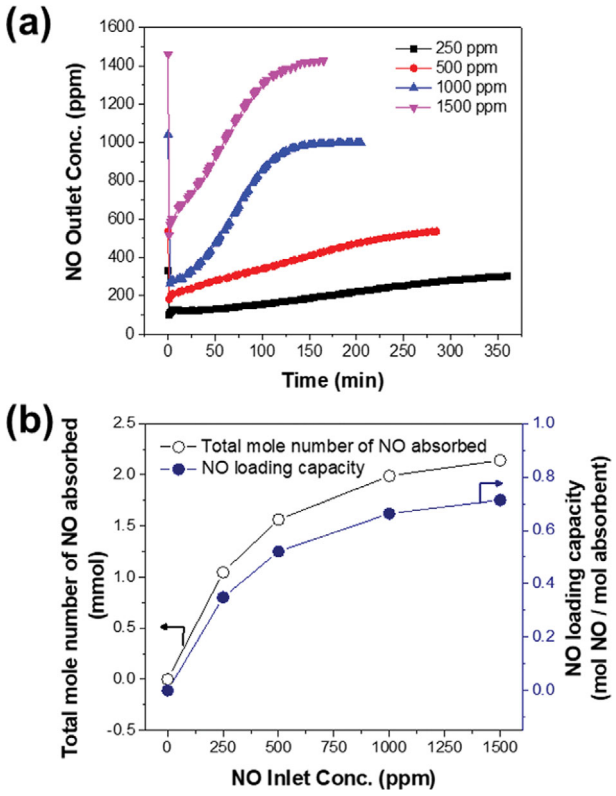


**Fig. 4. (a) NO outlet concentration profiles and, (b) Total mole number of the absorbed NO and NO loading capacity for different NO inlet concentration (Fe(II)EDTA$^{2-}$=10 mM, pH=6, V=300 ml).**

We also investigated effects of NO inlet concentrations on NO adsorption. Fig. 4(a) shows NO outlet concentration profiles when different NO inlet concentrations with identical Fe(II)EDTA$^{2-}$ concentration (10 mM) are introduced. When NO inlet concentration was relatively low at 250 ppm, the NO outlet concentration quickly decreased to 102 ppm. It then increased until reaching a saturation state. It took a relatively long time to achieve the saturation state. As NO inlet concentration increased to 500 ppm, the NO outlet concentration profile seemed to be similar to that of the 250 ppm one. It quickly decreased from 536 ppm to 182 ppm. It then increased to saturation state. For the 500 ppm case, it took a relatively shorter time to reach the saturation state compared to the 250 ppm case. As NO inlet concentrations increased, initial lowest NO outlet concentrations increased and the time to achieve saturation became even shorter.

We estimated the amount of total adsorbed NO by integrating the upper region of the curve of NO outlet concentration. Calculated amounts of total adsorbed NO were 1.05, 1.56, 1.99, and 2.14 mmol when inlet NO concentrations were 250, 500, 1,000, and 1,500 ppm, respectively. Similarly, NO loading capacity values were 0.35, 0.52, 0.63, and 0.71 mol NO/mol absorbent when inlet NO concentrations were 250, 500, 1,000, and 1,500 ppm, respectively (Fig. 4(b)). It is well known that a higher partial pressure of NO can induce a higher dissolved NO concentration at the gas-liquid interface based on Henry's Law as shown in the following equation [28]:

$$C_{NO,\ interface} = H_{NO} P_{NO} \quad (6)$$

When the inlet NO concertation is increased, it should show similar effect to increasing local partial pressure of NO at the gas-liquid interface in the absorption system. Thus, it should result in an increased concentration of dissolved NO in the adsorption solution, which should then induce an increase of NO concentration which can practically react with Fe(II)EDTA$^{2-}$. As mentioned, NO absorption reaction rate can be expressed $r = kC_{Fe(II)EDTA^{2-}} C_{NO}$ [20]. In the case of identical concentration of Fe(II)EDTA$^{2-}$ ($C_{Fe(II)EDTA^{2-}}$) is applied, the reaction rate is dependent on the concentration of NO ($C_{NO}$). Thus, higher gas-phase NO concentration should result in higher $C_{NO}$, it induces a larger liquid-gas phase absorption reaction rate [35]. As a result, the total mole number of NO absorbed was increased as the concentration of dissolved NO ($C_{NO}$) increased. In addition, NO loading capacity was increased when NO inlet concentration was increased. At equilibrium, K′ value became higher by K′=K*[NO] with increasing amount of dissolved NO. As a result, the NO loading capacity also tended to increase with increasing NO inlet concentration.

Fig. 5 shows NO outlet concentration profiles and NO loading capacity when the initial pH value of adsorption solution is varied. Previously, it has been reported that pH of absorption solution is an important parameter with a significant effect on NO absorption [20,21,36]. We carried out NO absorption by varying the initial solution pH from 2 to 10 and recorded the time to achieve

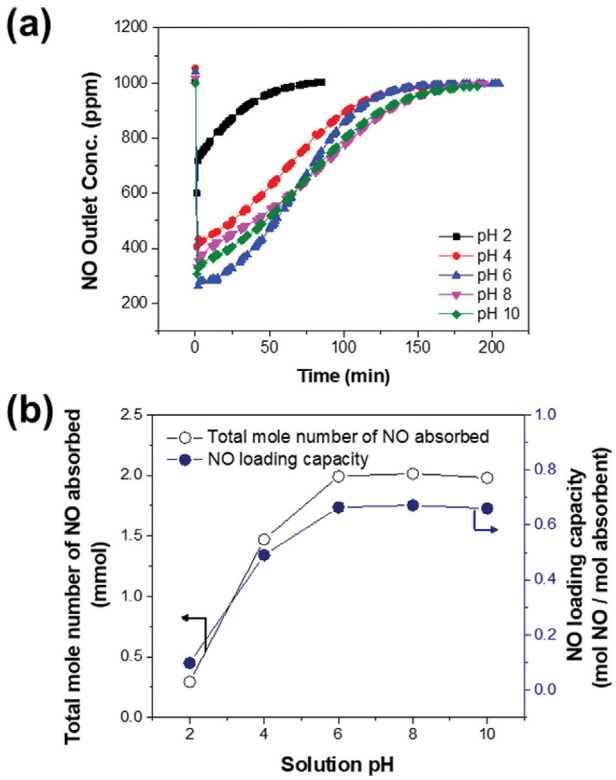


**Fig. 5. (a) NO outlet concentration profiles and, (b) Total mole number of the absorbed NO and NO loading capacity in different solution pH (NO inlet concentration=1,000 ppm, Fe(II)EDTA$^{2-}$ =10 mM, V=300 ml).**

the saturation point. As shown in Fig. 5(a), the lowest NO outlet concentration value quickly dropped from 1,003 ppm to 599 ppm and then increased when solution pH was 2. The shortest time to reach saturation was 82 min. As the solution pH increased from 2 to 4, the lowest NO outlet concentration point became much smaller compared to the one at pH 2. In addition, the time to reach the saturation point was significantly elongated. When we increased the pH value of the absorption solution to be even higher such as pH 6, the lowest NO outlet concentration was 262 ppm. It took the longest time to reach the saturation state. When the solution pH was increased further to 8 and 10, the lowest NO outlet concentration point and the time to reach saturation state showed similar profiles.

Fig. 5(b) shows amounts of total adsorbed NO and NO loading capacities when the initial pH value of adsorption solution is varied. When pH values of solution were pH 2, pH 4, pH 6, pH 8, and pH 10, amounts of total adsorbed NO were 0.29, 1.47, 1.99, 2.01, and 1.98 mmol, respectively. NO loading capacity showed a similar trend, with values of 0.098, 0.49, 0.66, 0.67, and 0.66 (mol NO/mol absorbent) for pH 2, pH 4, pH 6, pH 8, and pH 10, respectively. Note that the amount of total absorbed NO was the lowest at pH 2. It increased with increasing pH until pH 6. In addition, amounts of absorbed NO were similar in both neutral (pH 6 and 8) and alkaline (pH 10) environments. Messele et al. studied main chemical species at different pH when both Fe ions and EDTA ions are dissolved in an aqueous solution [37]. They reported that Fe(II)EDTA$^{2-}$ was one of the main species in aqueous solution with pH above 3. In acidic conditions (under pH 3), they found that Fe(II) ions existed without any chemical binding with other species. In addition, Fe-H-EDTA$^{-}$ was one of the chemical species in the solution. As pH increased to either neutral and alkaline condition, both Fe ions and EDTA ions easily formed Fe(II)EDTA$^{2-}$ species in the solution. Since the absolute amount of the formed Fe(II)EDTA$^{2-}$ was smaller in acidic conditions, the amount of NO adsorption was significantly lower. When pH was increased, Fe(II)EDTA$^{2-}$ started to form considerably from ca. pH 4. At neutral and alkaline conditions, all Fe ions and EDTA ions generated Fe(II)EDTA$^{2-}$ and the maximum amount of NO adsorption was achieved. Based on previous studies and our results, neutral and alkaline environments provide favorable conditions for formation of Fe(II)EDTA$^{2-}$, it could be concluded that solution pH must be maintained in a neutral or alkaline state, which is more advantageous for NO absorption by Fe(II)EDTA$^{2-}$ than an acid one.

**2. Simultaneous Absorption of NO and $SO_2$ Using Fe(II)EDTA$^{2-}$ Absorbent**

Generally, when fossil fuels such as coal, natural gases, and diesel are combusted, both toxic nitric oxides (NOx) and sulfur oxides ($SO_2$) are simultaneously generated [14,38-40]. Toxic chemicals including NOx and $SO_2$ must be removed before combustion flue gases are released to the atmospheric environment. We evaluated the performance for simultaneous removal of NO and $SO_2$. Fig. 6 summarizes results of simultaneous absorption of NO and $SO_2$. Fig. 6(a) shows NO inlet concentration profiles when different concentrations of $SO_2$ are simultaneously introduced into the absorption solution. The NO outlet concentration showed a similar behavior which quickly decreased to 82 ppm. It then increased until it reached a saturation state. All cases showed similar NO outlet concentration profiles. However, the NO loading capacity slightly increased when 175 ppm $SO_2$ was introduced (Fig. 6(b)). It is well known that introduction of a small amount of $SO_3^{2-}$ into the Fe(II)EDTA$^{2-}$ absorption solution has a positive impact on NO removal. He et al. reported that aqueous $SO_3^{2-}$ ions play a beneficial role in regeneration of both Fe(II)EDTA-NO$^{2-}$ and Fe(III)EDTA$^{-}$ to Fe(II)EDTA$^{2-}$ [20]. When $SO_2$ is introduced into the aqueous solution, $SO_2$ is converted to sulfite ion species. Dissolved sulfite ions species could reduce Fe(II)EDTA-NO$^{2-}$ to Fe(II)EDTA$^{2-}$ through the following chemical reactions. Thus, introducing $SO_2$ with a suitable concentration is helpful for NO absorption.

$$SO_2 + H_2O \rightarrow SO_3^{2-} + 2H^+ \quad (7)$$

$$Fe(II)EDTA\text{-}NO + SO_3^{2-} \rightarrow 2Fe(II)EDTA^{2-} + N_2O + SO_4^{2-} \quad (8)$$

As shown in Fig. 6(b), as the $SO_2$ inlet concentration increased to 350, 700, and 2,500 ppm, the NO loading capacity continuously decreased to 0.45, 0.42, and 0.40 (mol NO/mol absorbent), respectively. This could be explained by the following two reasons. As the amount of $SO_2$ dissolved increased, the solution pH dramatically decreased. When higher SOx concentration was introduced, a more rapid drop of solution pH was observed (Fig. 6(c)). As explained in Fig. 5, when a higher $SO_2$ concentration was introduced, the solution pH was changed to an acidic one, resulting in existence of Fe(II) ions without any chemical binding and formation of unfa-

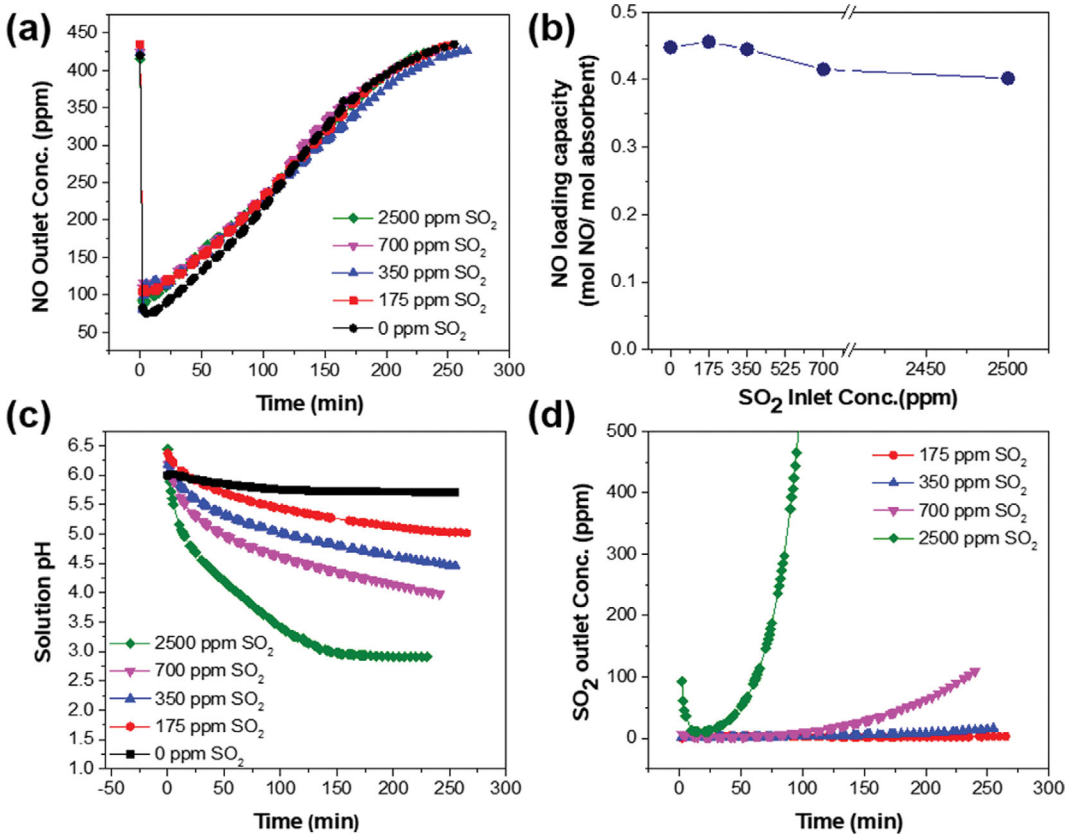


**Fig. 6. (a) NO outlet concentration profiles, (b) NO loading capacity, (c) solution pH and (d) $SO_2$ outlet concentration profiles for different $SO_2$ inlet concentration at 350 ppm NO in 10 mM Fe(II)$EDTA^{2-}$.**

**Table 2. Flue gas composition and parameters**

| References | NOx (ppm) | $SO_2$ (ppm) | $CO_2$ (vol%) | $O_2$ (vol%) | Generator |
|---|---|---|---|---|---|
| [39] | 200-300 | 100-200 | 13.5 | 11 | Laziska Power Plant |
| [40] | 100-200 | 150-400 | 9-12 | 4-8 | Typical flue gas |
| [38] | 237-410 | 260-457 | 12.5-14.5 | 5-6.5 | Coal fired power plant |

vorable Fe-H-$EDTA^-$. In addition, as the inlet concentration of $SO_2$ was extremely high compared to NO, the $SO_2$ could hinder NO molecules to contact Fe(II)$EDTA^{2-}$ at the gas-liquid interface. Thus, as the concentration of $SO_2$ introduced into the solution became higher, pH of absorption solution could be easily changed to acidic conditions, resulting in a relatively low degree of formation for Fe(II)$EDTA^{2-}$. In addition, the binding frequency between NO and Fe(II)$EDTA^{2-}$ at the gas-liquid interface was reduced.

As shown in Fig. 6(d), $SO_2$ outlet concentration was below 4 ppm for 265, 145, and 65 min when $SO_2$ inlet concentrations were 175, 350, and 700 ppm, respectively. It is well known that $SO_2$ absorption is sensitive to pH of absorption solution and that its absorption kinetics is dramatically decreased when the pH is below 4-5. As expected, when 175 ppm of $SO_2$ was used, the solution pH was maintained at above 5 and outlet $SO_2$ concentration was maintained at a low level (4 ppm) for the longest period until NO saturation was reached. However, when 350 ppm and 700 ppm of $SO_2$ were used, the $SO_2$ outlet concentrations were increased above 4 ppm when pH values of solution were slightly increased to be 4.82 and 4.85, respectively. When $SO_2$ is dissolved into an aqueous solution followed by generation of sulfite ions, by-product hydrogen ions ($H^+$) are generated, resulting in an acidic environment (Eq. (8)). Since it is well known that $SO_2$ absorption is also unfavorable below pH 5, acidic conditions can prevent rapid $SO_2$ absorption, resulting in relatively high $SO_2$ outlet concentrations. When we introduced an extremely high concentration of $SO_2$ (2,500 ppm), solution pH dramatically dropped to be below pH 5 within 20 min and the $SO_2$ outlet concentration was easily increased within a short period of time (ca. 20 min).

Table 2 summarizes emission concentrations of NO, $SO_2$, and $O_2$ from various plants based on previous references. It can be seen that emissions appeared in various ranges depending on fuels and combustion conditions of plants. Note that NO emission ranges were in the concentration range of 200-500 ppm and $SO_2$ emission ranges were in the range of 100 to 800 ppm. It is well known that $O_2$ concentration in flue gases is about 5-6 vol%. Thus, we used a model flue gas stream with the following inlet concentration for the next experiment: 350 ppm NO, 350 ppm $SO_2$, and 5 vol% $O_2$.

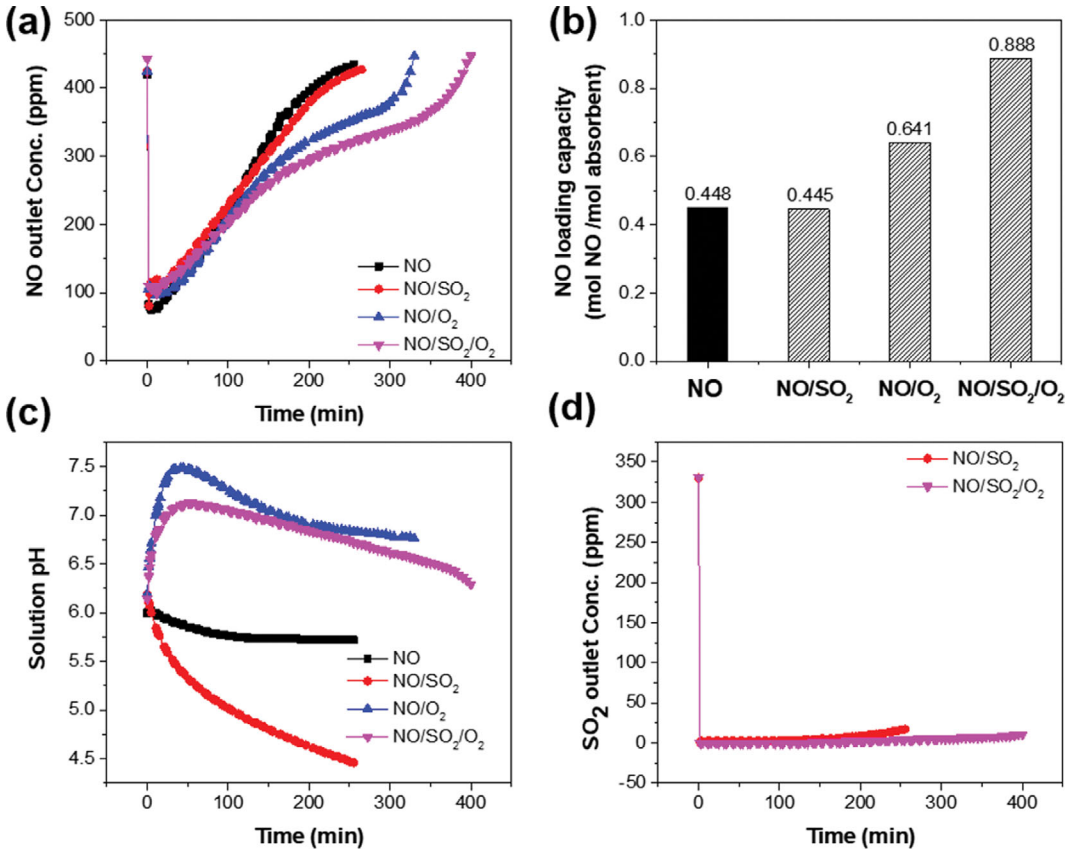


**Fig. 7. (a) NO outlet concentration profiles, (b) NO loading capacity, (c) solution pH and (d) $SO_2$ outlet concentration profiles of model flue gas component (NO=350 ppm, $SO_2$=350 ppm, $O_2$=5%) in 10 mM Fe(II)EDTA$^{2-}$.**

We additionally conducted NO, $SO_2$ absorption with $CO_2$ in $O_2$ environments. It can be seen that $CO_2$ concentration in flue gases is about 9-14.5 vol%. We used 350 ppm NO, 350 ppm $SO_2$ 12 vol% $CO_2$. 5% $O_2$ for the NO/$SO_2$/$CO_2$/$O_2$ inlet concentration.

Fig. 7 summarizes results of simultaneous absorption of NO and $SO_2$ in the presence of components of the model flue gas. Fig. 7(a) shows the NO inlet concentration profile when different combinations of gas components (NO only, NO/$SO_2$, NO/$O_2$, and NO/$SO_2$/$O_2$) are introduced. All cases show similar lowest NO concentration (81-110 ppm) and similar recovery patterns until saturation. When only NO gas was introduced into the absorption solution, typical NO outlet concentration profiles were obtained in which NO outlet concentration dropped to the lowest value followed by increasing until it reached the saturation state. In case of NO with $SO_2$ used, NO outlet concentration profiles seemed to be almost identical to the case of NO only. When NO was introduced with 5 vol% $O_2$, NO outlet concentration profiles were slightly changed after 150 min. In the presence of $O_2$, both cases of NO with $O_2$ and NO with both $SO_2$ and $O_2$ showed gently changed slope of NO outlet concentration, indicating that NO absorption continued. Practically, it should be noted that the time to reach saturation time was longer. Fig. 7(b) shows NO loading capacity values when different combinations of gas components are introduced. NO loading capacity values were 0.448, 0.445, 0.641 and 0.888 (mol NO/mol absorbent) for NO, NO/$SO_2$, NO/$O_2$, and NO/$SO_2$/$O_2$, respectively.

When only NO gas was introduced (NO), the dominant reaction in the absorption solution was chemical binding between Fe(II)EDTA$^{2-}$ and NO at the gas-liquid interface (Eq. (2)). Thus, the amount of NO adsorbed and the NO loading capacity were dependent on concentrations of both Fe(II)EDTA$^{2-}$ and NO. When NO with $SO_2$ was introduced (NO/$SO_2$), $SO_2$ was converted to sulfite species in aqueous solution, resulting in reduction of Fe(II)EDTA-NO$^{2-}$ and Fe(III)EDTA$^-$ to Fe(II)EDTA$^{2-}$. Although sulfite can recover all Fe(II)EDTA-NO$^{2-}$ and Fe(III)EDTA$^-$ to Fe(II)EDTA$^{2-}$, the solution is changed to an acidic environment, which is an unfavorable condition for the formation of Fe(II)EDTA$^{2-}$ as $SO_2$ is continuously dissolved. Thus, it slightly lowers the NO loading capacity (0.445 mol NO/mol adsorbent) compared to NO (0.448 mol NO/mol absorbent). It is well known that Fe(II)EDTA$^{2-}$ can be easily oxidized to Fe(III)EDTA$^-$ in the presence of oxygen (Eq. (10)). Since Fe(III)EDTA$^-$ does not have any affinity toward NO, oxidation of Fe(II)EDTA$^{2-}$ to Fe(III)EDTA$^-$ must be avoided. In this work, we used enough L-Ascorbic acid as a reducing agent. We should reduce Fe(III)EDTA$^-$ to Fe(II)EDTA$^{2-}$ and prevent oxidation of Fe(II)EDTA$^{2-}$ to Fe(III)EDTA$^-$ (Eq. (11)). In addition, NO can be oxidized to $NO_2$ in the presence of $O_2$. $NO_2$ can then be converted into $NO_2^-$ and $NO_3^-$ forms in an aqueous solution (Eqs. (12), (13), and (14)). Thus, since NO could be absorbed into water as a form of $NO_3^-$ in the presence of oxygen, it seems that the NO loading capacity is significantly increased.

$$Fe(II)EDTA^{2-} + O_2 + 4H^+ \rightarrow 4Fe(III)EDTA^- + 2H_2O \quad (9)$$

$$C_6H_8O_6 + 2Fe(III)EDTA^- \rightarrow 2Fe(II)EDTA^{2-} + C_6H_6O_6 + 2H^+ \quad (10)$$

$$2NO(g) + O_2 \rightarrow 2NO_2(g) \quad (11)$$

$$2NO_2(aq) + H_2O \rightarrow 2H^+ + NO_2^- + NO_3^- \quad (12)$$

$$2Fe(II)EDTA^{2-} + NO_2^- + 2H^+ \rightarrow Fe(II)EDTA\text{-}NO^{2-} + Fe(III)EDTA^- + H_2O \quad (13)$$

$$2Fe(II)EDTA\text{-}NO^{2-} + 2Fe(II)EDTA^{2-} + 4H^+ \rightarrow 4Fe(III)EDTA^- + N_2 + 2H_2O \quad (14)$$

When all components (NO, $SO_2$, and $O_2$) are introduced into the Fe(II)EDTA$^{2-}$ absorbent solution, a complicated reaction could occur and an antagonistic effect on NO absorption might appear, resulting in dramatically high NO loading capacity (NO/$SO_2$/$O_2$). As shown in Fig. 7(c), when $O_2$ was introduced (NO/$O_2$ and NO/$SO_2$/$O_2$), the solution pH was increased from pH 6 to pH 7-7.5. It was then maintained in the range of neutral pH conditions. According to Eq. (10), the pH of the absorption solution increased in the presence of $O_2$ because $H^+$ ions were consumed for oxidation of Fe(II)EDTA$^{2-}$. At the same time, $H^+$ ions were continuously generated through dissolution of $SO_2$ followed by formation of sulfite ions, resulting in decreased solution pH. Thus, the pH should be maintained in a neutral environment so that Fe(II)EDTA$^{2-}$ can well exist in the solution. In addition, since sulfite ions can play an important role in regeneration of Fe(II)EDTA$^{2-}$, they can maintain a high concentration of Fe(II)EDTA$^{2-}$, resulting in a positive effect on NO absorption. As shown in Fig. 7(d), $SO_2$ outlet concentration was well maintained below 10 ppm for 400 min when all components (NO, $SO_2$, and $O_2$) were introduced. As mentioned, $SO_2$ absorption is highly influenced by solution pH and a high $SO_2$ absorption will occur when the absorption solution has a neutral pH. Therefore, it can be concluded that antagonistic effects of $SO_2$ and $O_2$ in NO/$SO_2$/$O_2$ can significantly influence absorption conditions, resulting in excellent NO and $SO_2$ absorption performance.

We additionally carried out absorption of NO and $SO_2$ in presence of either $CO_2$ or $O_2$ environments. Fig. S1 compares the results of simultaneous absorption of both NO and $SO_2$ in presence of either $CO_2$ or $O_2$ by using Fe(II)EDTA$^{2-}$ absorbent. As shown in Fig. S1(a), NO outlet concentration profile of presence of $O_2$ (NO/$SO_2$/$O_2$) is a similar pattern to that of presence of both $CO_2$ and $O_2$ (NO/$SO_2$/$CO_2$/$O_2$), even though the former has minor longer absorption performance. Fig. S1(b) shows NO loading capacity values when different combinations of gas components (NO/$SO_2$/$O_2$ or NO/$SO_2$/$CO_2$/$O_2$) are introduced. NO loading capacity value was 0.888 and 0.813 (mol NO/mol absorbent) for NO/$SO_2$/$O_2$ or NO/$SO_2$/$CO_2$/$O_2$ introduced. When multiple gas components are introduced to absorption media, it is well known that the competition dissolution can occur, resulting in low absorption capacity. Thus, when a gas stream of NO/$SO_2$/$CO_2$/$O_2$ is introduced, the amount of NO dissolved could be slightly low compared to case of NO/$SO_2$/$O_2$. In addition, when $CO_2$ is introduced to aqueous solution, pH of solution is significantly influenced. As mentioned in Figs. 5 to 7, the solution pH significantly influences NO/$SO_2$ absorption capacity. As shown in Fig. S1(c), when a gas stream of NO/$SO_2$/$CO_2$/$O_2$ is used, the solution pH is maintained at 5.67-6.14 until NO reaches the saturation state. Based on the carbonate system (Eqs. (15)-(18)), aqueous $CO_2$ can form carbonic acid ($H_2CO_3$) and then first proton is released to form bicarbonate ($HCO_3^-$). It is well known that bicarbonate ions have great buffer effect by either releasing or capturing $H^+$ ions up to ca pH 6.3. When $CO_2$ is dissolved, carbonic acid releases $H^+$ ions, resulting in that pH slightly drops, then bicarbonate ions act as buffer chemical inducing that pH is maintained in the range of 6-6.3 (Fig. S1(c)). Although Fe(II)EDTA$^{2-}$ can catch NO when pH is well maintained about 6, both neutral and slightly weak base (pH 8) is more beneficial to absorb NO using Fe(II)EDTA$^{2-}$ solution as shown in Fig. 5. Therefore, NO loading capacity of gas stream of NO/$SO_2$/$CO_2$/$O_2$ was slightly lower than that of gas stream of NO/$SO_2$/$O_2$. $SO_2$ absorption is also highly influenced by solution pH. Therefore, $SO_2$ outlet concentration was well maintained below 10 ppm until NO reached the saturation state since pH is maintained is around pH 6.1.

$$CO_2(g) \leftrightarrow CO_2(L) \quad (15)$$

$$CO_2(L) + H_2O \leftrightarrow H_2CO_3 \quad (16)$$

$$H_2CO_3 + H_2O \leftrightarrow HCO_3^- + H^+ \quad (17)$$

$$HCO_3^- \leftrightarrow CO_3^{2-} + H^+ \quad (18)$$

## CONCLUSIONS

We investigated effects of various parameters on simultaneous removal of NO and $SO_2$ using Fe(II)EDTA$^{2-}$ absorbent in a lab scale reactor. Effects of various parameters, such as Fe(II)EDTA$^{2-}$ concentration, solution volume, NO Inlet concentration, and pH of absorption solution on NO absorption, were investigated. In addition, we evaluated absorption profiles of NO and $SO_2$ over Fe(II)EDTA$^{2-}$ in model flue gas flow. We systematically obtained absorption performance results toward both NO and $SO_2$. Conclusions are shown below:

1. NO loading capacity is significantly influenced by operation parameters such as Fe(II)EDTA$^{2-}$ concentration, solution pH, and NO inlet concentration in wet NO absorption. Although both Fe(II)EDTA$^{2-}$ concertation and solution volume were varied, the NO loading capacity was almost identical. However, the NO loading capacity was increased when both solution pH and inlet NO concentration were increased.
2. During simultaneous removal of NO and $SO_2$, $SO_2$ had a positive effect on absorption solution. It could induce regeneration of Fe(II)EDTA-NO$^{2-}$ and Fe(III)EDTA$^-$ to Fe(II)EDTA$^{2-}$. However, when a high concentration of $SO_2$ was introduced into the solution, larger amounts of $H^+$ ions were generated during dissolution of $SO_2$. It induced an unfavorable condition for formation of Fe(II)EDTA$^{2-}$ and the dissolved $SO_3^{2-}$ ions hindered NO from contacting Fe(II)EDTA$^{2-}$, resulting in a low NO loading capacity.
3. To investigate the absorption of NO in the flue gas component emitted from an actual plant, NO and $SO_2$ in presence $O_2$ were introduced into the Fe(II)EDTA$^{2-}$ absorption solution. Antagonistic effects of $SO_2$ and $O_2$ could significantly influence absorption conditions, resulting in a high NO loading capacity of about 0.888 mol NO/mol absorbent.

## ACKNOWLEDGEMENTS

This research was also supported by the Ministry of Environment's Fine Dust Blind Spots Reduction Program (KEITI No. 2020003060005).

## SUPPORTING INFORMATION

Additional information as noted in the text. This information is available via the Internet at http://www.springer.com/chemistry/journal/11814.

## REFERENCES

1. D. Kang and J.-E. Kim, *J. Korean Med. Sci.*, **29**(5), 621 (2014).
2. V. V. Tran, D. Park and Y.-C. Lee, *Int. J. Environ. Res. Public Health*, **17**(8), 2927 (2020).
3. G. Qi and R. T. Yang, *J. Catal.*, **217**(2), 434 (2003).
4. D. Ren, K. Gui, S. Gu and Y. Wei, *J. Alloys Compd.*, **867**, 158787 (2021).
5. Y. Wang, H. Li, S. Wang, X. Wang, Z. He and J. Hu, *Fuel Process. Technol.*, **188**, 179 (2019).
6. S. W. Bae, S. A. Roh and S. D. Kim, *Chemosphere*, **65**(1), 170 (2006).
7. V. M. Zamansky, V. V. Lissianski, P. M. Maly, L. Ho, D. Rusli and W. C. Gardiner Jr., *Combust. Flame*, **117**(4), 821 (1999).
8. H. H. Kim, G. Prieto, K. Takashima, S. Katsura and A. Mizuno, *J. Electrost.*, **55**(1), 25 (2002).
9. I. Nakamura, N. Negishi, S. Kutsuna, T. Ihara, S. Sugihara and K. Takeuchi, *J. Mol. Catal. A Chem.*, **161**(1-2), 205 (2000).
10. P. van der Maas, L. Harmsen, S. Weelink, B. Klapwijk and P. Lens, *J. Chem. Technol. Biotechnol.*, **79**(8), 835 (2004).
11. A. Abdulrasheed, A. Jalil, S. Triwahyono, M. Zaini, Y. Gambo and M. Ibrahim, *Renew. Sust. Energy Rev.*, **94**, 1067 (2018).
12. J. Xu, G. Chen, F. Guo and J. Xie, *Chem. Eng. J.*, **353**, 507 (2018).
13. M. Q. Peng, R. Zhao, M. Xia, C. J. Li, X. L. Gong, D. Wang and D. S. Xia, *Fuel*, **200**, 290 (2017).
14. S. M. Ma, Y. C. Zhao, J. P. Yang, S. B. Zhang, J. Y. Zhang and C. G. Zheng, *Renew. Sust. Energy Rev.*, **67**, 791 (2017).
15. B. Yan, J. Yang, M. Guo, G. Chen, Z. Li and S. Ma, *J. Ind. Eng. Chem.*, **20**(4), 2528 (2014).
16. F. He, Y. Qian and J. Xu, *Energy Fuels*, **33**(4), 3331 (2019).
17. Y. Duo, X. Wang, J. He, S. Zhang, H. Pan, J. Chen and J. Chen, *Environ. Sci. Pollut. Res.*, **26**(28), 28808 (2019).
18. F. He, X. Deng and M. Chen, *Fuel*, **199**, 523 (2017).
19. X. Zhu, F. He, M. Xia, H. Liu and J. Ding, *RSC Adv.*, **9**(42), 24386 (2019).
20. F. He, X. Zhu, X. Chen and J. Ding, *Fuel*, **284**, 119070 (2021).
21. Y. G. Adewuyi and M. A. Khan, *Chem. Eng. J*, **304**, 793 (2016).
22. Y. G. Adewuyi and M. A. Khan, *Chem. Eng. J*, **281**, 575 (2015).
23. T. T. Suchecki, B. Mathews and H. Kumazawa, *Ind. Eng. Chem. Res.*, **44**(12), 4249 (2005).
24. J. R. Yan, F. X. Zhou, Y. Zhou, X. H. Wu, Q. L. Zhu, H. Y. Liu and H. F. Lu, *Environ. Technol. Inno.*, **11**, 41 (2018).
25. P. Van der Maas, P. Van den Brink, S. Utomo, B. Klapwijk and P. Lens, *Biotechnol. Bioeng.*, **94**(3), 575 (2006).
26. E. Narita, T. Sato, T. Shioya, M. Ikari and T. Okabe, *Ind. Eng. Chem. Res. Dev.*, **23**(2), 262 (1984).
27. S. Wang, Q. Zhang, G. Zhang, Z. Wang and P. Zhu, *J. Energy Inst.*, **90**(4), 522 (2017).
28. T. W. Chien, H. T. Hsueh, B. Y. Chu and H. Chu, *Process Saf. Environ. Prot.*, **87**(5), 300 (2009).
29. E. Sada, H. Kumazawa, I. Kudo and T. Kondo, *Ind. Eng. Chem. Process. Des. Dev.*, **20**(1), 46 (1981).
30. J. Han, X. Yao, L. Qin, M. Jiang, F. Xing and W. Chen, *Int. J. Environ. Res.*, **10**(4), 519 (2016).
31. W. Jiang, X. Wang, Q. Xu, J. Xiao and X. Wei, *RSC Adv.*, **9**(1), 132 (2019).
32. M. X. Chen, J. T. Zhou, Y. Zhang, X. J. Wang, Z. Shi and X. W. Wang, *World J. Microb. Biot.*, **31**(3), 527 (2015).
33. X. Y. Dong, Y. Zhang, J. T. Zhou, M. X. Chen, X. J. Wang and Z. Shi, *Bioresour. Technol.*, **138**, 339 (2013).
34. E. Sada, H. Kumazawa, I. Kudo and T. Kondo, *Ind. Eng. Chem. Process. Des. Dev.*, **19**(3), 377 (1980).
35. Y. G. Adewuyi and N. Y. Sakyi, *Ind. Eng. Chem. Res.*, **52**(41), 14687 (2013).
36. N. Liu, B.-H. Lu, S.-H. Zhang, J.-L. Jiang, L.-L. Cai, W. Li and Y. He, *Energy Fuels*, **26**(8), 4910 (2012).
37. S. A. Messele, C. Bengoa, F. E. Stuber, J. Giralt, A. Fortuny, A. Fabregat and J. Font, *Catalysts*, **9**(5), 474 (2019).
38. I. Aouini, A. Ledoux, L. Estel and S. Mary, *Oil Gas Sci. Technol.*, **69**(6), 1091 (2014).
39. L. Więcław-Solny, A. Tatarczuk, M. Stec and A. Krótki, *Energy Procedia*, **63**, 6318 (2014).
40. F. Scala, A. Lancia, R. Nigro and G. Volpicelli, *J. Air Waste Manage. Assoc.*, **55**(1), 20 (2005).

## Supporting Information

# Effects of operation conditions on absorption of nitric oxide and sulfur oxide using Fe(II)EDTA$^{2-}$ absorbents

**Yoon Hee Kim*, Jiyull Kim*, Na Yeon Kim*, Dong Seop Choi*, Dong Hun Lee*, Eunju Yoo*, Young Eun Kim*, Jongwon Choi**, and Ji Bong Joo*,†**

*Department of Chemical Engineering, Konkuk University, 120 Neungdong-ro, Gwangjin-gu, Seoul 05029, Korea
**Korea Institute of Energy Research (KIER), 152, Gajeong-ro, Yuseong-gu, Daejeon 34129, Korea
(*Received 29 October 2022 • Revised 13 December 2022 • Accepted 20 December 2022*)

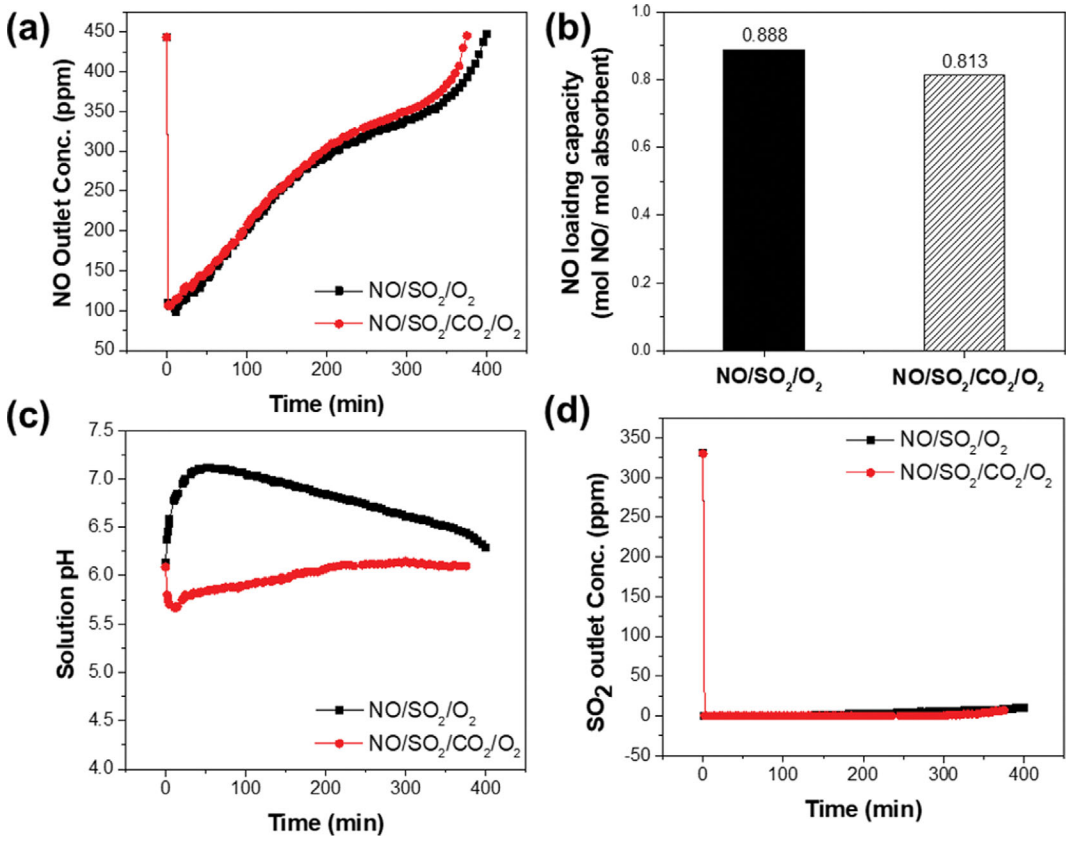


**Fig. S1. (a) NO concentration profiles, (b) NO loading capacity, (c) solution pH and (d) $SO_2$ concentration profiles of $NO/SO_2/CO_2/O_2$ (NO= 350 ppm, $SO_2$=350 ppm, $CO_2$=12%, $O_2$=5%) in 10 mM Fe(II)EDTA$^{2-}$.**